Nonlocal electrodynamics in Weyl semi-metals

B. Rosenstein,[1,2] H.C. Kao,[3] and M. Lewkowicz[2]

[1]*Electrophysics Department, National Chiao Tung University, Hsinchu 30050, Taiwan, R. O. C.*
[2]*Physics Department, Ariel University, Ariel 40700, Israel*
[3]*Physics Department, National Taiwan Normal University, Taipei 11677, Taiwan, R. O. C.*

(Dated: August 10, 2015)

Recently synthesized 3D materials with Dirac spectrum exhibit peculiar electric transport qualitatively different from its 2D analogue, graphene. Neglecting impuritiy scattering, the real part of the conductivity is strongly frequency dependent (linear), while the imaginary part is non-zero (unlike in undoped, clean graphene). The Coulomb interaction between electrons is unscreened as in a dielectric and hence is long range. We demonstrate that the interaction correction renders the electrodynamics nonlocal on a mesoscopic scale. The longitudinal conductivity σ_L (related by charge conservation to the electric susceptibility) and the transverse conductivity σ_T are different in the long wave length limit and consequently the standard local Ohm's law description does not apply. This leads to several remarkable effects in transport and optical response. We predict a charging effect in DC transport that is a direct signature of the nonlocality. The optical response of the WSM is also sensitive to the nonlocality. In these materials p-polarized light generates bulk plasmons as well as the transversal waves. The propagation inside the WSM is only slightly attenuated. At a specific (material parameter dependent) frequency the two modes coincide, a phenomenon impossible in a local medium. Remarkably, for any frequency there is an incident angle where total absorption occurs, turning the WSM opaque.

PACS numbers:

One of the common assumptions of electrodynamics in electrically active media is that the effect of external electric fields can be described *locally* by constitutive relations connecting the "induced" currents to the electric field even when spatial dispersion is present. Generally, due to space - time translational symmetry of the material, the relation between Fourier components (ω is the frequency, $\mathbf{k}$ the wavevector) of the electric field and these of the induced current density within linear response reads:

$$J_i(\omega,\mathbf{k}) = \sigma_{ij}(\omega,\mathbf{k})\, E_j(\omega,\mathbf{k}). \tag{1}$$

Here σ is the AC conductivity tensor with indices $i,j = x,y,z$. The locality of the electrodynamic response in Fourier space means that the long wavelength limit exists: $\sigma_{ij}(\omega,\mathbf{k}=\mathbf{0}) \equiv \sigma_{ij}(\omega)$. The conductivity tensor for a homogeneous, isotropic, space and time-reversal invariant (nongyrotropic) material at $\mathbf{k}=\mathbf{0}$ simplifies into the simple form of Ohm's law:

$$\sigma_{ij}(\omega) = \delta_{ij}\sigma(\omega), \tag{2}$$

or $\mathbf{J}(\omega) = \sigma(\omega)\,\mathbf{E}(\omega)$.

On the microscopic level the locality is not guaranteed[1]. It hinges on the nature of the charges in the condensed matter system and presence of long-range interaction between them. These in turn determine the long-wave excitations of the material. In an insulator (or semiconductor at low temperatures) locality is simply a result of absence of gapless charged excitations. This does not apply to metals.

In the free electron gas model of an ideal metal, i.e. neglecting both disorder and electron-electron interactions, there is no energy gap, so there are gapless charged excitations. The conductivity tensor in a metal can be uniquely decomposed into a transversal and a longitudinal part (assuming rotational and reflection symmetry for simplicity)[1]:

$$\sigma_{ij}(\omega,\mathbf{k}) = \left(\delta_{ij} - \frac{k_i k_j}{k^2}\right)\sigma_T(\omega,\mathbf{k}) + \frac{k_i k_j}{k^2}\sigma_L(\omega,\mathbf{k}), \tag{3}$$

Yet, the standard 'Lindhard' type calculations in an absolutely clean metal with an arbitrary dispersion relation of the charge carriers and *finite area* Fermi surface, see Fig.1a, show that the two scalars σ_T and σ_L are not independent at small wavevectors,

$$\begin{aligned} \sigma_T(\omega,\mathbf{k}=\mathbf{0}) &= \sigma_L(\omega,\mathbf{k}=\mathbf{0}) \equiv \sigma(\omega); \\ \sigma_L(\omega,\mathbf{k}) - \sigma_T(\omega,\mathbf{k}) &= \beta(\omega)\,k^2 + O\left(k^4\right), \end{aligned} \tag{4}$$

thus leading to the local Ohm's law Eq.(2).

Impurities in a metal also define a length scale, the mean free path, that effectively makes the carriers' motion diffusive and the charge excitations "massive" in terms of their dispersion relation. Accounting for impurities within the self consistent harmonic approximation (yet still neglecting Coulomb interactions) thus makes the long wavelength limit of the Lindhard diagram smooth[2]. Beyond the harmonic approximation, composite excitations like diffusons have zero modes. However coupling of the external fields to these excitations is "soft" enough to cause the so-called "infrared divergencies" that in principle could make the long wavelength limit singular [2].

Returning to a very clean electron gas, the nonlocality can in principle arise due to long-range Coulomb interactions. However, long-range interactions are not screened only in insulators. In a metallic state with finite density of charges (finite density of states on the Fermi surface) the nonlocality is prevented by the screening of the Coulomb force that becomes effectively short-range and thus unable to cause infrared divergencies. As a result clean interacting charged electron gas is local.

All the above reasons ensuring locality, namely a direct energy gap, significant disorder and screening of the Coulomb interactions, are inapplicable to the recently discovered Weyl semi-metals (WSM). In these crystals electronic states are described by the Bloch wave functions, obeying the 3D "pseudo-relativistic" Weyl (Dirac) equation with Fermi velocity v replacing the velocity of light, see Fig.1b. The novelty of the physics of WSM at Dirac point is clearly due to its "ultrarelativistic" dispersion, $\varepsilon_{\mathbf{k}} = vk$, of the elementary excitations. The Fermi level at neutrality point is occupied by a finite number of states (zero density of states), so that the excitations are those of the neutral plasma.

Although the two-band electronic structure of bismuth was described by a four-component nearly massless Dirac fermion in 3D caused by spin-orbit interaction long ago [3] (with spin replacing pseudospin), only recently several systems were experimentally demonstrated to exhibit the 3D Dirac quasiparticles. Materials are quite diverse and include the time - reversal invariant topological Dirac semimetal [4, 5] Na_3Bi (predicted[7, 8]), a bulk crystal symmetry protected semimetal[6, 9] Cd_3As_2 with a single pair of Dirac points [10], crystals on the phase transition boundary between topological and band insulators $HgCdTe$[11]. Recently, Weyl semi-metals exhibiting Fermi arcs on their surface were discovered[12–14]. All these materials exhibit a great variety of new electromagnetic transport and optical phenomena (not seen even in 2D WSM like graphene) including giant diamagnetism, quantum magnetoresistance showing linear field dependence[15–18], superconductivity[19] *etc.*

There is no finite energy gap in WSM to ensure locality as in band insulators or semiconductors. In this paper we assume that the WSM is clean enough, so that the disorder scale is irrelevant and the chemical potential is tuned to the Dirac point. The elementary excitations are still "massless" at long wavelengths like in a metal. To no surprise the free (noninteracting) electron gas AC conductivity of WSM, calculated recently[20, 21], turned out to remain local (see discussion below). However calculating the screening due to the interaction corrections[20, 22, 23], it became clear that the Coulomb interactions are still long range (namely like an insulator WSM is unable to screen the Coulomb interactions, unlike in the metal). The reason for locality mentioned with respect to metals therefore does not apply. So that there is no good reason to exclude the possibility that the long-wave electric response of WSM in the presence of strong interactions is nonlocal. To summarize WSM exhibits a curious mixture of properties usually attributed either to metals or insulators that does not allow to apply a conventional reasoning to establish locality of the linear response.

In the present paper we demonstrate by explicit microscopic calculation of the interaction effects in a rather generic model of WSM that the electrodynamics is indeed nonlocal. The rather unusual macroscopic electrodynamics then is formulated and applied to various physical phenomena. Several experimental setups in which the nonlocality can be demonstrated are suggested. These include the charging effects in DC transport, while another is the optical generation of both longitudinal (plasmon) and transversal waves in these materials and their subsequent propagation.

RESULTS

The model

An analogous calculation in graphene[26, 27] (a 2D version of WSM) reveals that in order to avoid complications linked to the absence of scale separation in the system of relativistic massless fermions (known otherwise as "anomaly"), one should use a well defined lattice model. Electrons in WSM are described sufficiently accurately for our purposes by the tight binding model of nearest neighbors on a cubic lattice[20, 28] $\mathbf{n} = n_i\mathbf{a}_i$ (see Fig.2a). The Hamiltonian is

$$\widehat{K} = \frac{i\gamma}{2}\sum_{n,i} c^{\alpha\dagger}_{\mathbf{n}}\sigma^{\alpha\beta}_i c^{\beta}_{\mathbf{n}+\mathbf{a}_i} + hc, \tag{5}$$

where σ_i are Pauli matrices, operators $c^{\alpha\dagger}_{\mathbf{n}}$, $\alpha = 1, 2$, create a two - component spinor (describing two orbitals per site) and γ is the hopping energy determining the Fermi velocity $v = \gamma a/\hbar$ (a - lattice spacing). This defines a propagator depicted by arrows (see Fig.2b) in the Feynman diagrams. The Coulomb interaction (neglecting retardation effects) on the lattice can be viewed as an exchange of static photons. In term of Fourier components it takes the form (see[29] for details)

$$\widehat{V} = \frac{1}{2\mathcal{V}}\sum_{\mathbf{pkl}} v_{\mathbf{p}} c^{\sigma\dagger}_{\mathbf{k}+\mathbf{p}} c^{\sigma}_{\mathbf{k}} c^{\rho\dagger}_{\mathbf{l}-\mathbf{p}} c^{\rho}_{\mathbf{l}}, \tag{6}$$

where $\mathcal{V}$ is the sample volume and

$$v_{\mathbf{p}} = \frac{\pi e^2}{\sin^2(p_x a/2) + \sin^2(p_y a/2) + \sin^2(p_z a/2)}. \tag{7}$$

The photon propagator $v_{\mathbf{p}}$ is represented by wavy lines in Fig.2.

It is convenient to calculate the transverse and longitudinal conductivities from the scalar quantities using $\sigma_L = k_i k_j \sigma_{ij}/k^2$ and $\sigma_{ii} = 2\sigma_T + \sigma_L$. The relations follow from Eq.(3). The calculation involves evaluation of diagrams 2c for free electrons and 2d, 2e, 2f for the leading interaction corrections, self energy, the vertex renormalization and "glasses" diagram, respectively. Details involving renormalization, cancellation of both infrared and ultraviolet divergences appear in the Supplementary Information SI1, while results are given Eq.(8) and Eq.(11).

The electrodynamics of a free Fermi gas is local

The dispersive conductivity tensor for a free (neglecting the electron-electron interaction) clean ultrarelativistic fermion gas at Dirac point is (see [29]):

$$\sigma_{ij}(\omega,\mathbf{k}) = \frac{Ne^2}{24\pi\hbar v\omega}\left(1-\frac{i}{\pi}\log\frac{\Lambda^2 v^2}{\omega^2-v^2k^2}\right)\left\{\delta_{ij}\left(\omega^2-v^2k^2\right)+v^2k_ik_j\right\}. \quad (8)$$

N is the number of Weyl fermions and $\Lambda \sim 1/a$ is the ultraviolet cutoff. In the long wavelength limit one recovers the AC conductivity $\sigma^0_{ij}(\omega,\mathbf{k}=\mathbf{0}) = \sigma_0(\omega)\delta_{ij}$ with

$$\sigma_0(\omega) = \frac{Ne^2\omega}{24\pi\hbar v}\left(1-\frac{i}{\pi}\log\frac{\Lambda^2v^2}{\omega^2}\right). \quad (9)$$

This has both a real and an imaginary part, logarithmically divergent as function of Λ. Thus the DC conductivity is zero, i.e. the material behaves like an insulator, qualitatively different from graphene that is a pseudo-dissipative metal. This already indicates that in 3D the Coulomb interaction is unscreened[20]. The dependence on the wave vector follows uniquely from the pseudo- relativistic invariance of the free Weyl gas like in its 2D analogue, graphene [27]. Hence, using notations of Eq.(4), the electrodynamics is local with

$$\beta^0(\omega) = -\frac{\sigma_0(\omega)v^2}{\omega^2}. \quad (10)$$

Interactions cause nonlocal electrodynamics

Using the Coulomb interaction Hamiltonian within the tight binding model, Eq.(6), one obtains the corrections to first order in the effective interaction strength $\alpha = e^2/\kappa\hbar v$, where κ denotes the dielectric constant of the background. While the corrections to either σ_T or σ_L are small, the relative correction to the difference $\sigma_{nl} \equiv \sigma_L - \sigma_T$ is actually dominant for $\mathbf{k}=\mathbf{0}$ and can be considerable in the homogenous regime $v^2k^2 << \omega^2$. While in free WSM $\sigma_{nl}(\omega,\mathbf{0})$ was zero, now it becomes finite:

$$\sigma_{nl}(\omega,\mathbf{0}) = \sigma_0(\omega)\left\{\frac{\pi\alpha}{3}\log\frac{0.6\omega^2}{\overline{\omega}^2}+O\left(\alpha^2\right)\right\}. \quad (11)$$

Here $\overline{\omega}$ is the frequency at which the renormalized value of the (renormalization group "running") Fermi velocity $v(\overline{\omega})$ and the renormalized coupling $\alpha = \alpha(\overline{\omega})$ are defined[20, 22, 23]. Details of the calculation are given in [29].

Optics/Plasmonics within WSM

Let us now develop the equations for the electromagnetic fields on the macroscopic scale in a WSM. We employ the Landau-Lifshitz[30, 31] definition of the macroscopic fields

$$\begin{aligned}\nabla\cdot\mathbf{D} &= 4\pi\rho_{ext}; \quad \nabla\times\mathbf{E} = -\frac{1}{c}\dot{\mathbf{B}}; \quad (12)\\ \nabla\cdot\mathbf{B} &= 0; \quad \nabla\times\mathbf{B} = \frac{1}{c}\left(\dot{\mathbf{D}}+4\pi\mathbf{J}_{ext}\right).\end{aligned}$$

The displacement field is $\mathbf{D} = \mathbf{E}+4\pi\mathbf{P}$, where the polarization vector is defined by $\dot{\mathbf{P}} = \mathbf{J}$. The induced current Eq.(1) is determined nonlocally by the conductivity tensor given in Eqs.(10) and (11). In particular, for the harmonic dependence $\mathbf{E}(\mathbf{r},t) = \mathbf{E}_0 e^{i(\mathbf{k}\cdot\mathbf{r}-\omega t)}$ (and without external charges and currents) Gauss' Law demands that either $\mathbf{E}$ is transversal, $\mathbf{k}\cdot\mathbf{E}=0$, or else the dispersion relation is plasmonic:

$$1+i\frac{4\pi}{\omega}\sigma_L(\omega,\mathbf{k}) = 0. \quad (13)$$

Ampère's Law together with Faraday's Law results in the condition that either $\mathbf{E}$ is longitudinal, $\mathbf{k}\times\mathbf{E}=\mathbf{0}$, or the dispersion relation is transversal:

$$1+i\frac{4\pi}{\omega}\sigma_T(\omega,\mathbf{k}) = \frac{c^2k^2}{\omega^2}. \quad (14)$$

It is interesting to note that when $\omega << \Lambda v$ the conductivity, Eq.(10) is approximately purely imaginary and one obtains the dispersion relations for the longitudinal ("plasmon", wavevector $\mathbf{q}$), and transversal ("light", wavevector $\mathbf{p}$), waves :

$$q^2 = \frac{\omega^2}{v^2}\left\{1+\left(1+\frac{N\alpha}{24\pi}\log\frac{\Lambda^2v^2}{\omega^2}\right)^{-1}+\frac{\pi\alpha}{3}\log\frac{0.6\omega^2}{\overline{\omega}^2}\right\}; \quad (15)$$

$$p^2 = \frac{\omega^2}{c^2}\left\{1+\frac{1+\frac{N\alpha}{24\pi}\log\left(\Lambda^2v^2/\omega^2\right)}{1+\frac{v^2}{c^2}\frac{N\alpha}{24\pi}\log\left(\Lambda^2v^2/\omega^2\right)}\right\}. \quad (16)$$

The results for q, p in units of $\overline{\omega}/v$ as functions of $\omega/\overline{\omega}$ in the case of $N = 4$, $v(\overline{\omega}) = c/300$, $\alpha(\overline{\omega}) = 0.2$, $\hbar v\Lambda = 5eV$, (characteristic of Na_3Bi and Cd_3As_2 for $\overline{\omega}$ in the THz range) are presented in Fig. 3. One observes that the light wavevector $\mathbf{p}$ is real for all frequencies, that is the wave is nondissipating, see the left inset in Fig.3a. The plasmon wave vector $\mathbf{q}$ is real, according to Eq.(15), only above a certain threshold frequency ω_p, see Fig.3b. One should emphasize that the "plasma frequency" is that of a neutral plasma rather than that of the charged plasma in metals. However within the renormalized perturbation theory used to derive the equation, the low frequency region might be unreliable. Above the threshold the two waves coexist and both wavevectors are real.

In local materials equations Eq.(16) and Eq.(15) cannot be satisfied by the same wave vector: the difference of the equations is $i\frac{4\pi}{\omega}\sigma_{nl}(\omega,\mathbf{q}_m) = -c^2k^2/\omega^2$. Using $\sigma_{nl}(\omega,\mathbf{k}) = -\beta_0(\omega)k^2$,see Eq.(10), this leads to $4\pi i\omega\beta_0(\omega) = c^2$ that generally cannot be satisfied. In WSM, on the other hand, $\sigma_{nl}(\omega,\mathbf{0})$ is finite and determines the special value of the wave vector at which both transverse and longitudinal waves are the same. We further discuss this in the optical set up. Next we suggest two potential experimental setups that demonstrate the nonlocality of the WSM electrodynamics.

Reflection and refraction on a dielectric - WSM interface

Let's consider the following setup, see Fig.4. An electromagnetic wave with the wavevector $k_x > 0, k_y = 0$ and $k_z < 0$ is incident at the angle θ with the normal on a semi-infinite WSM. The electric field with p - polarization in vacuum is then described by a superposition of incoming and reflected waves:

$$E_i^{vac} = A\left\{\frac{k_z}{k},0,\frac{-k_x}{k}\right\}e^{i(k_xx+k_zz)} - B\left\{\frac{k_z}{k},0,\frac{k_x}{k}\right\}e^{i(k_xx-k_zz)} \quad (17)$$

where A is the incoming and B the reflected amplitude, respectively. The field in the WSM is given by

$$E_i = C_T\left\{\frac{p_z}{p},0,\frac{-k_x}{p}\right\}e^{i(k_xx+p_zz)} + C_L\left\{\frac{k_x}{q},0,\frac{q_z}{q}\right\}e^{i(k_xx+q_zz)}, \quad (18)$$

where C_T and C_L are the transmitted transversal and longitudinal amplitudes.

Employing the Landau-Lifshitz notation for the macroscopic fields in Maxwell equations in dispersive media Eq.(12), used by Golubkov[31] to resolve similar problems as in exciton physics[32], the list of the continuity conditions on the boundary is:

(i) the normal component of $\mathbf{D}$:

$$E_z^{vac} = \frac{4\pi i}{\omega}\sigma_{zx}E_x^{wsm} + \left(1+\frac{4\pi i}{\omega}\sigma_{zz}\right)E_z^{wsm}.$$

(ii) the tangential component of $\mathbf{E}$: $E_x^{vac} = E_x^{wsm}$.

(iii) the normal component of $\mathbf{B}$: $\partial_xE_y^{vac} = \partial_xE_y^{wsm}$.

(iv) the tangential component of $\mathbf{B}$: $\partial_zE_x^{vac} - \partial_xE_z^{vac} = \partial_zE_x^{wsm} - \partial_xE_z^{wsm}$.

(v) In addition, since two different modes propagate in the bulk one needs a so-called ABC (additional boundary condition)[32, 33]. Assuming a "sharp" interface (width smaller than the wavelength) the simplest ABC suffices:

$$J_z(z=0) = 0 \to \sigma_{zx}E_x^{wsm} + \sigma_{zz}E_z^{wsm} = 0.$$

This reflects the fact that the electric current cannot escape the material.

Applying these boundary conditions we obtain the following reflection and transmission amplitudes:

$$r = \frac{1-D}{1+D}; t_T = \frac{2k/p}{1+D}; \quad t_L = -\frac{2k_xq\left(p^2-k^2\right)}{kq_zp^2(1+D)}; \quad D = \frac{k^2p_zq_z - \left(p^2-k^2\right)k_x^2}{k_zq_zp^2}. \quad (19)$$

When $D = 1$ the reflection coefficient vanishes and total absorption occurs, thus turning the WSM opaque at frequency-dependent incident angles.

The s - polarization does not generate a plasmon. The amplitudes are standard: $r = (1-p_z/k_z)/(1+p_z/k_z)$ and $t = 2/(1+p_z/k_z)$. In Fig.5a the amplitudes for the p-polarizations (solid) and the s-polarizations (dashed)

are presented. Fig.5b shows the vanishing of the p-polarization reflection coefficient at various incident angles in the THz range.

Surface charging due to DC current

Two possible experiments are suggested for low frequency transport in WSM. A Corbino geometry is employed in order to avoid ambiguities related to boundaries, see Figs.6 and 7. A slowly alternating flux is generated by a thin solenoid inserted into the cylindrical aperture (radius R) inside a sufficiently large WSM sample. The fluxon's magnetic field is linear in time (at times smaller than $1/\omega$). Within that period of time the associated electric fields in the aperture and the WSM are time independent. In the first setup the fluxon is concentrated at distance d from the center: $\Phi(\mathbf{r},t) = \Phi_0 \omega t \delta(\mathbf{r} - d\hat{\mathbf{x}})$. The solenoidal part of the electric field produced by the fluxon is

$$E_i^{sol}(\mathbf{r}) = \frac{\omega \Phi_0}{2\pi b^2} \varepsilon_{ij} b_j, \tag{20}$$

where $\mathbf{b} = \mathbf{r} - d\hat{\mathbf{x}}$, $i, j = x, y$. It induces currents in the WSM that in turn generate charge distributions on the aperture surface, provided that the flux is not concentric with the cylinder axis. The surface charge density $Q(\phi)$ is obtained from the condition that the normal component of the current on the surface on the semimetal side vanishes, $\mathbf{n} \cdot \mathbf{J} = \mathbf{0}$. The irrotational part of the electric field is

$$E_i^{irr}(\mathbf{r}) = L \int_{\phi=0}^{2\pi} \int_z \frac{s_i \, Q(\phi)}{\left(z^2 + s^2\right)^{3/2}}, \tag{21}$$

where the distance from a point on the surface to the observation point $\mathbf{r}$ is denoted by $\mathbf{s} = \mathbf{r} - R\mathbf{n}'$. The boundary condition, $\mathbf{n} \cdot \mathbf{J} = \mathbf{n} \cdot \left(\sigma_T \mathbf{E}^{sol} + \sigma_L \mathbf{E}^{irr}\right) = 0$, together with Gauss's Law, $\mathbf{n} \cdot \mathbf{E}^{irr} = 2\pi Q(\phi)$, leads to a dipole-like charge density. The details of the calculation are given in [34]. The surface charge density as a function of the polar angle ϕ is

$$Q(\phi) = \frac{\sigma_T}{\sigma_L} \omega \Phi_0 \frac{d \sin\phi}{4\pi^2 \left(R^2 - 2Rd\cos\phi + d^2\right)}. \tag{22}$$

The dominant linear ω dependence of the conductivities cancels in the ratio $\frac{\sigma_T}{\sigma_L} = 1 - \frac{\pi\alpha}{3} \log \frac{0.6\omega^2}{\overline{\omega}^2}$. The surface charge can be measured by gauging the electric field near the interior surface of the material. The deviation of σ_T/σ_L from unity (the value in the case of a local conductor) is an indicator of nonlocality of electrodynamics. Note that a central position of the fluxon would not induce the surface charges. The distribution of charge is given in Fig. 6b.

for surface charging due to DC current, the calculation is more complex since induced charges appear not only on the aperture surface, but also on the

For the second experimental setup, see Fig. 7 involve a Corbino disk with the fluxon in the center of a composite cylinder of WSM ($0 < \phi < \pi$) and a usual "local" conductor (for example semiconductor) in the lower segment $\pi < \phi < 2\pi$; surface charges are now induced at the interfaces $\phi = 0$ and π between the two materials which in turn cause surface charges at the aperture. This results in an integral equation that fortunately can be solved exactly, see [34], and results in

$$Q(\phi) = \frac{\sigma - \sigma_T}{\sigma + \sigma_L} \frac{\omega \Phi_0}{(2\pi)^3 R} \log \frac{1 + \cos\phi}{1 - \cos\phi}. \tag{23}$$

The distribution of this surface charge density is shown in Fig.7.

DISCUSSION

The calculation of the leading Coulomb interaction effect on the electromagnetic response of 3D Weyl semimetal reveals that its macroscopic electrodynamics becomes nonlocal in a sense that the wave vector dependent AC conductivity tensor becomes nonanalytic at small wave vectors, see Eq.(3). The origin of nonlocality is a unique combination of the long - range (unscreened) Coulomb interactions like in dielectrics and the ultra - relativistic nature of the quasiparticles. The longitudinal conductivity σ_L (related by charge conservation to the electric susceptibility) and the transverse conductivity σ_T are different in the long wave length limit and consequently the standard local Ohm's law description does not apply.

Several experimental signatures of the nonlocal contribution to conductivity, Eq.(11) were pointed out. After reformulating the macroscopic electrodynamics in terms of the longitudinal and transverse fields with corresponding material parameters, the charging effect in DC transport in Corbino geometry was worked out. The set up avoids potential complications with conventional leads and contacts, while allowing for an unambiguous indication of nonzero difference $\sigma_{nl} = \sigma_L - \sigma_T$. A more conventional set up is the measurement of optical response of the WSM that is also sensitive to the nonlocality. The p-polarized light at general frequency ω generates in these materials besides the transversal waves also the longitudinal one (that can be viewed as a charge density wave or a bulk plasmon). The propagation inside the WSM is only slightly attenuated, so that one can measure both the reflection and two transmission amplitudes, all dependent on σ_{nl}. At a specific (material parameter dependent) frequency the two modes coincide, a phenomenon impossible in a local medium. The polarization dependence of

the light reflection (transmission) off a WSM slab is sensitive to both σ_L and σ_T. Remarkably for any frequency there exists an incident angle where total absorption occurs, so that WSM is opaque.

The applicability of perturbation theory in 3D Weyl semi-metals was quite recently addressed by several groups who used renormalization group and other non-perturbative methods like the random phase and large N approximations[23, 35, 36]. The latter shows perturbation theory to be reliable over a wide range of values of the interaction strength α, up to a critical value $\alpha_c \approx 14$. In addition, typical values of the background dielectric constant in 3D WSM in the range $\kappa \sim 20 - 40$ have been measured[23], which assures a below the critical value of the interaction strength. In contrast, in the 2D case, where a critical value $\alpha_c = 0.78$ was found[37], the situation for perturbation theory is less fortunate since the measurement on samples substrated on boron nitride or on suspended samples provided values close to that[38, 39].

Acknowledgements. We are indebted to W.B. Jian, I. Herbut, E. Farber, C. W. Luo, D. Cheskis. Work of H.K. was supported by NSC of R.O.C. Grants101-2112-M-003-002-MY3.

[1] Giuliani, G. and Vignale, G. *Quantum Theory of the Electron Liquid.* (Cambridge University Press, Cambridge, 2005).

[2] Rammer, J. *Quantum Transport Theory* . (Perseus Books, Reading MA, 1998).

[3] Wolff, P.A. Matrix elements and selection rules for the two-band model of bismuth. *J. Phys. Chem. Sol.* **25,** 1057 (1964).

[4] Liu, Z.K. et al. Discovery of a Three-Dimensional Topological Dirac Semimetal, Na_3Bi. *Science* **343,** 864 (2014).

[5] Kushwaha, S.K. et al. Bulk crystal growth and electronic characterization of the 3D Dirac semimetal Na_3Bi. *APL Mat.* **3,** 041504 (2015).

[6] Liu, Z.Q. et al. A stable three-dimensional topological Dirac semimetal Cd_3As_2. *Nature Mater*ials **13,** 677 (2014).

[7] Wang, Z., Weng, H., Wu, Q., Dai, X. and Fang, Z. Three-dimensional Dirac semimetal and quantum transport in Cd_3As_2. *Phys. Rev. B* **88,** 125427 (2013).

[8] Wang, Z. et al. Dirac semimetal and topological phase transitions in A_3Bi $(A = Na, K, Rb)$. *Phys. Rev. B* **85,** 195320 (2012).

[9] Xu, G., Weng, H., Wang, Z., Dai, X. and Fang, Z. Chern Semimetal and the Quantized Anomalous Hall Effect in $HgCr_2Se_4$. *Phys. Rev. Lett.* **107,** 186806 (2011).

[10] Neupane, M., et.al. Observation of a topological 3D Dirac semimetal phase in high-mobility Cd_3As_2. *Nature Commun.* **05,** 3786 (2014).

[11] Orlita M. et al.. Observation of the 3D massless Kane fermions observed in a zinc-blende crystal. *Nature Phys.* **10,** 233 (2014).

[12] Lv, B.Q. et al. Discovery of Weyl semimetal $TaAs$. arXiv:1502.04684 [cond-mat.mtrl-sci].

[13] Lv, B.Q. et al. Observation of Weyl nodes in $TaAs$. arXiv:1503.09188 [cond-mat.mtrl-sci].

[14] Xu, S.Y. et al. Discovery of Weyl semimetal $NbAs$. arXiv:1504.01350 [cond-mat.mes-hall].

[15] Kariyado, T. and Ogata, M. Three-Dimensional Dirac electrons at the Fermi energy in cubic inverse Perovskites: Ca_3PbO and its family. *J. Phys. Soc. Jpn.* **80**, (2011).

[16] Kariyado, T. and Ogata, M. Low-Energy Effective Hamiltonian and the Surface States of Ca_3PbO. *J. Phys. Soc. Jpn.* **81**, 064701 (2012).

[17] Xiong, J. et al. Anomalous conductivity tensor in the Dirac semimetal Na_3Bi. arXiv:1502.06266 [cond-mat.str-el].

[18] Liang,T. et.al. Ultrahigh mobility and giant magnetoresistance in the Dirac semimetal Cd_3As_2. *Nature Mater*ials **14,** 280 (2015).

[19] Wang, H. et al. Shuang Jia, Observation of superconductivity in 3D Dirac semimetal Cd_3As_2 crystal. arXiv:1501.00418 [cond-mat.supr-con].

[20] Rosenstein, B. and Lewkowicz, M. Dynamics of electric transport in interacting Weyl semimetals. *Phys. Rev. B* **88**, 045108 (2013).

[21] Lv M. and Zhang, S.C. Dielectric function, Friedel oscillations and plasmons in Weyl semimetals. *Int. J. Mod. Phys. B* **27,** 1250177 (2013).

[22] Hosur, P., Parameswaran S. A. and Vishwanath A. Charge transport in Weyl semimetals. *Phys. Rev. Lett.* **108,** 046602 (2012).

[23] Throckmorton, R.E., Hofmann, J., Barnes, E., and Das Sarma, S. Many-body effects and ultraviolet renormalization in 3D Dirac materials. arXiv:1505.05154 [cond-mat.mes-hall].

[24] Zivitz, M. and Stevenson, J.R. Optical properties of the $Cd_3As_2 - Cd_3P_2$ semiconductor alloy system. *Phys. Rev. B* **10,** 2457 (1974).

[25] Jay-Gerin, J.P., Aubin, M.J. and Caron, L.G. The electron mobility and the static dielectric constant of Cd_3As_2 at $4.2K$. *Solid State Communications* **21,** 771 (1977).

[26] Rosenstein, B., Maniv, T. and Lewkowicz, M. Chiral anomaly and strength of the electron-electron interaction in graphene. *Phys. Rev. Lett.* **110,** 066602 (2013).

[27] Rosenstein, B., Kao, H.C. and Lewkowicz, M. Long-range electron-electron interactions in graphene make its electrodynamics nonlocal. *Phys. Rev. B* **90,** 045137 (2014).

[28] Mastropietro, V. Interacting Weyl semimetals on a lattice. *J. Phys. A: Math. Theor.* **47,** 465003 (2014).

[29] Supplementary Information 1: The calculation of the interaction corrections to conductivity of WSM is outlined.

[30] Landau, L.D., Lifshitz, E.M. and Pitaevskii, L.P. *Electrodynamics of Continuous Media* (Elsevier Butterworth-Heinemann, Oxford, 1984).

[31] Golubkov, A.A. and Makarov, V.A. Boundary conditions for electromagnetic field on the surface of media with weak spatial dispersion. *Uspekhi Fizicheskikh Nauk* **38,** 325 (1995).

[32] Agranovich, V. M. and Ginzburg, V.L. *Crystal Optics with Spatial Dispersion, and Excitons* (Springer Verlag, Berlin, 1984).

[33] Pekar, S.I. The theory of electromagnetic waves in a crystal in which excitons are produced. *Sov. Phys. JETP* **6,** 785 (1958).

[34] Supplementary Information 2: The details of the calcu-

lation of the charging effect on the aperture surface.

[35] Gonzalez, J. Marginal Fermi liquid versus excitonic instability in three-dimensional Dirac semimetals. *Phys. Rev. B* **90,** 121107(R) (2014).

[36] Isobe, H. and Nagaosa, N. Renormalization group study of electromagnetic interaction in multi-Dirac-node systems. *Phys. Rev. B* **87,** 205138 (2013).

[37] Barnes, E., Hwan, E.H., Throckmorton, R.E., and Das Sarma, S. Effective field theory, three-loop perturbative expansion, and their experimental implications in graphene many-body effects. *Phys. Rev. B* **89,** 235431 (2014).

[38] Siegel, D.A. et al. Many-body interactions in quasi-freestanding graphene. *Proc. Nat. Acad. Sci. USA* **108,** 11365 (2011).

[39] Yu, G.L. et al. Interaction phenomena in graphene seen through quantum capacitance. *Proc. Nat. Acad. Sci. USA* **110,** 3282 (2013).

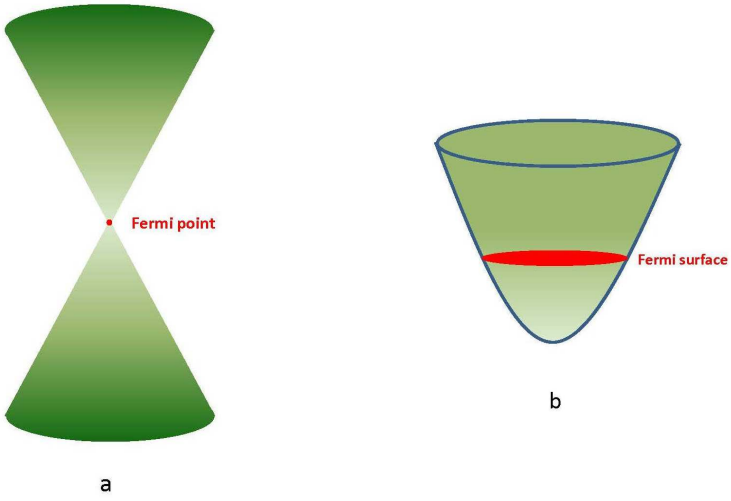

FIG. 1: Spectrum of a charged metal contrasted to that of a Weyl semimetal.
a. The Fermi level surface area is nonzero for a metal (or a band semimetal). The density of states at the Fermi level is finite (charged plasma) as is the density of charge carriers.
b. In a Weyl semimetal at neutrality (Dirac) point the Fermi level crosses the spectrum at finite number of states, so that the Fermi level surface area is zero. The electron gas constitutes a neutral plasma.

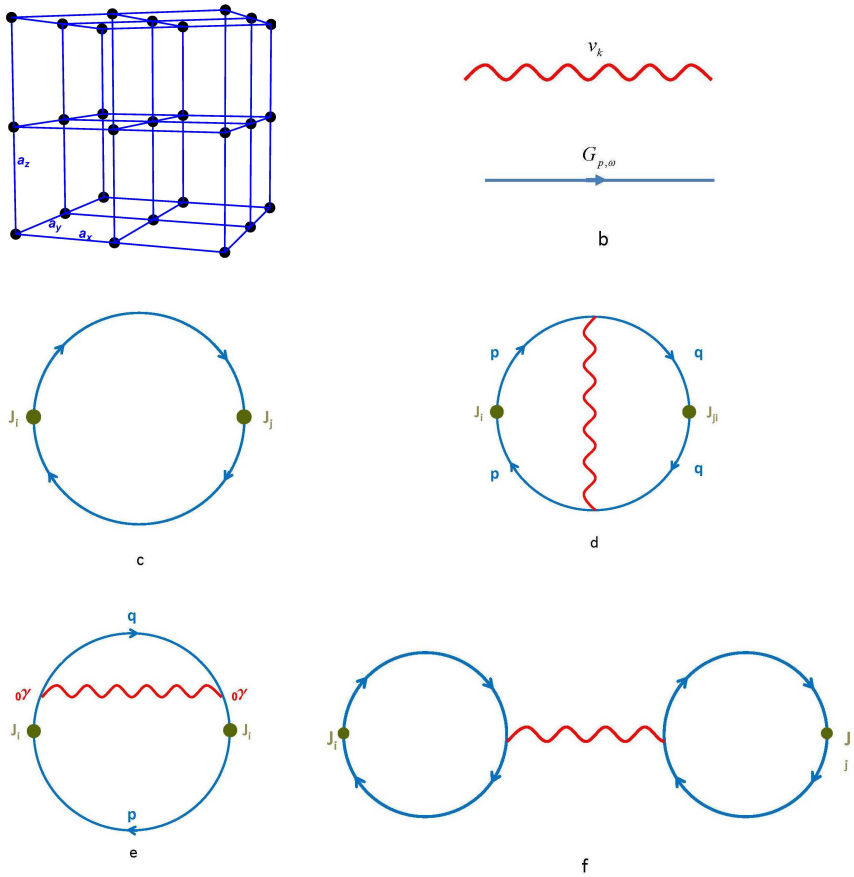

FIG. 2: The tight binding model and Feynman diagrams for conductivity tensor.
a. The cubic lattice.
b. Propagators and Coulomb interaction.
c. The leading order conductivity.
d. The vertex correction.
e. The self energy correction.
f. The "glasses" diagram.

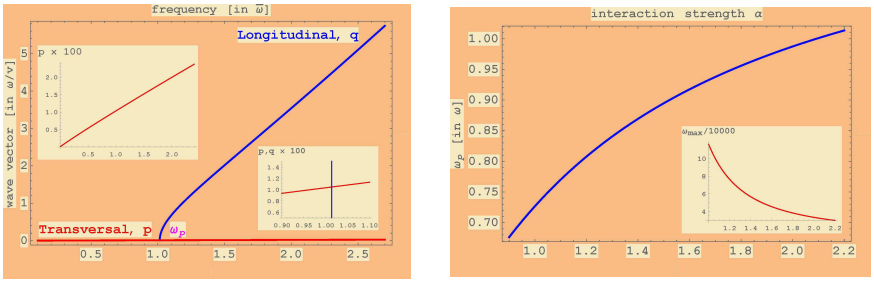

FIG. 3: Two branches of excitations in neutral plasma of the isotropic Weyl semimetal.
a. The transverse (red) and longitudinal (blue) wave vectors are monotonically increasing as function of frequency. At the intersection point at $\{q_m, \omega_m\}$ the electromagnetic wave is monochromatic (lower right insert).
b. The lower limiting (plasma) frequency at which the longitudinal wave appears as a function of the interaction strength α. The insert shows the upper limiting frequency.

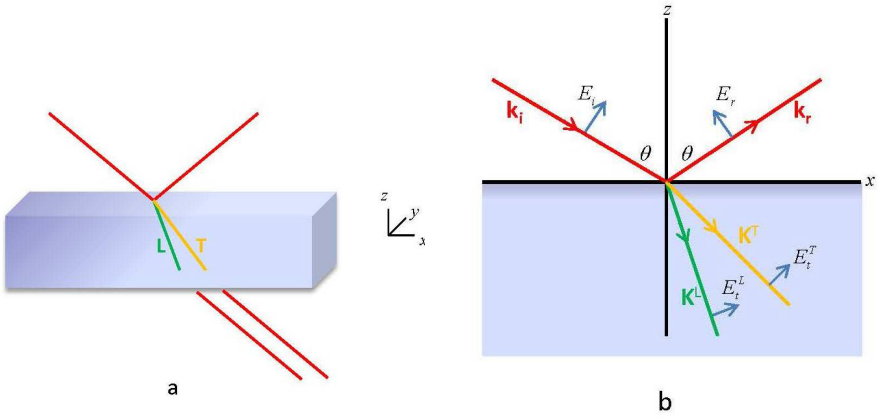

FIG. 4: Transmission and reflection of light in Weyl semimetal.
a. The light beam is either reflected or transmitted inside the WSM, where it splits into a longitudinal (green) and a transverse (yellow) mode.
b. The p-polarized light incident monochromatic beam with wave vector $\mathbf{k}$ incident at angle θ is split in the WSM into longitudinal (green) and transverse (yellow) modes with wave vectors $\mathbf{q}$ and $\mathbf{p}$, respectively. Directions of the electric fields are shown in blue.

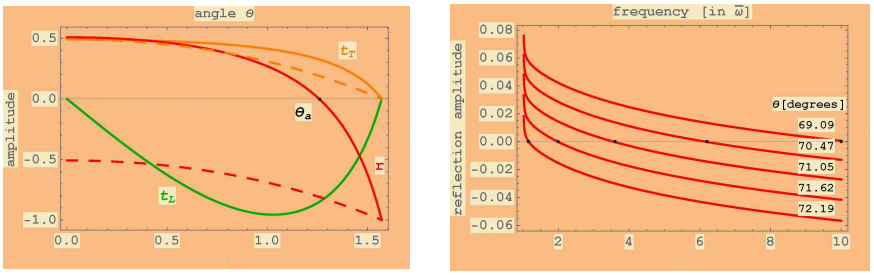

FIG. 5: Transmission and reflection of light in Weyl semimetal.
a. Reflection and transmission amplitudes as function of the incident angle θ. The p-polarization amplitudes (solid): reflected (red), transmitted transversal (yellow) and longtudinal (green); the incident radiation is totally absorbed at the interface at angle θ_a. The s-polarization amplitudes are plotted dashed.
b. The (p) reflection amplitude r as function of frequency for various incident angles displaying the total absorption.

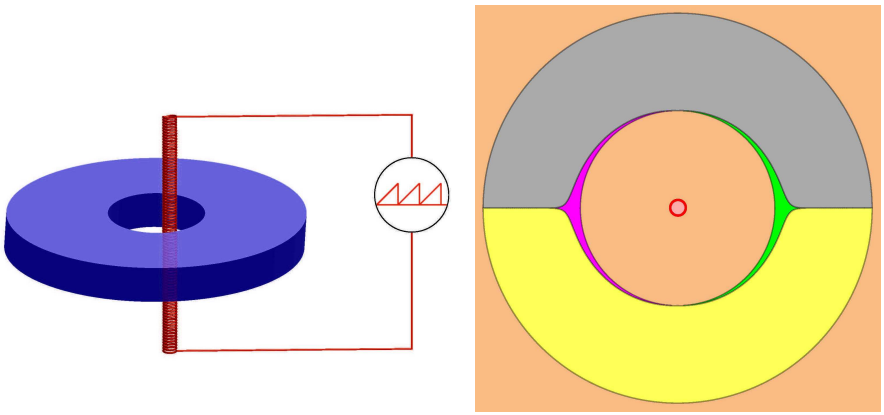

FIG. 6: Transmission and reflection of light in Weyl semimetal.
a. A thin solenoid inserted at distance d from the center of a hollow Weyl semimetal cylinder demonstrates the charging effect. The solenoid generates pulses of magnetic flux. During the pulse the internal surface of the aperture of radius R gets charged.
b. Charging effect in a system combining WSM and a conductor. The upper segment is a WSM, while the lower is an ordinary 'local' conductor (a semiconductor or a metal). The solenoid is placed in the center of the aperture. Charges appear both on the internal surface and interfaces. The surface charge density 23 as function of polar angle with $d/R = 1/2$.

Part I
Supplemental Information 1

1 Calculation of the interaction corrections to conductivity of WSM

1.1 The current density in the tight binding model

The minimal substitution determines the coupling of the external electromagnetic field, described by vector potential A_i with electrons on the lattice:

$$\widehat{K}_{mc}\left[A\left(r,t\right)\right]=\frac{i}{2}\sum_{n,i}\Gamma_{\mathbf{n},i}c_{\mathbf{n}}^{\alpha\dagger}\sigma_{i}^{\alpha\beta}c_{\mathbf{n}+\mathbf{a}_{i}}^{\beta}+hc, \tag{SI1(1)}$$

where the hopping integral $\Gamma_{\mathbf{n},i}$ becomes

$$\Gamma_{\mathbf{n},i}=\gamma\exp\left\{i\frac{ea}{c\hbar}\int_{s=0}^{1}A_{i}\left(\mathbf{n}+s\mathbf{a}_{i},t\right)\right\}. \tag{SI1(2)}$$

Applying the charge symmetry transformation $c_{n}^{\alpha}\rightarrow e^{i\chi_{n}(t)}c_{n}^{\alpha}$ the current density on the link is

$$J_{\mathbf{n}i}\left(t\right)\equiv-c\frac{\delta}{\delta A_{\mathbf{n}i}\left(t\right)}\widehat{K}_{mc}. \tag{SI1(3)}$$

In linear response the current density operator is expanded up to the first order in $A_{\mathbf{n}i}$ as $J_{\mathbf{n}i}\left(t\right)=J_{\mathbf{n}i}^{p}\left(t\right)+J_{\mathbf{n}i}^{d}\left(t\right)$:

$$\begin{aligned}J_{\mathbf{n}i}^{p}\left(t\right) &= \frac{ev}{2\hbar}c_{\mathbf{n}}^{\alpha\dagger}\sigma_{i}^{\alpha\beta}c_{\mathbf{n}+\mathbf{a}_{i}}^{\beta}+hc\\ J_{\mathbf{n}i}^{d}\left(t\right) &= i\frac{e^{2}va}{2c\hbar^{2}}\int_{s=0}^{1}A_{i}\left(\mathbf{n}+s\mathbf{a}_{i},t\right)c_{\mathbf{n}}^{\alpha\dagger}\sigma_{i}^{\alpha\beta}c_{\mathbf{n}+\mathbf{a}_{i}}^{\beta}+hc,\end{aligned} \tag{SI1(4)}$$

Normalized operators in momentum space are $c_{\mathbf{n}}^{\alpha}=\mathcal{N}^{-1/2}\sum_{\mathbf{k}}e^{-i\mathbf{k}\cdot\mathbf{n}}c_{\mathbf{k}}^{\alpha}$, where the number of unit cells is $\mathcal{N}=\mathcal{V}/a^{3}$ with $\mathcal{V}=a^{3}\sum_{\mathbf{n}}1$, where $\widehat{k}_{i}=\sin\left(ak_{i}\right)$. There are eight Weyl points at which $\varepsilon_{\mathbf{k}}=\left|\widehat{\mathbf{k}}\right|=0$ inside the Brillouin zone. The calculation therefore was performed for $N=8$.

1.2 Matsubara Action and Feynman rules

It is useful to represent the electron gas via the Matsubara action ($\tau = it$) involving the $3+1$ Fermion field ψ and the static photon (auxiliary) field ϕ :

$$A = \sum_{\mathbf{n}} \int_{\tau} \left\{ \begin{array}{c} \psi^{\dagger}_{\mathbf{n}}(\tau) \left(\frac{d}{d\tau} - ie\phi_{\mathbf{n}} \right) \psi_{\mathbf{n}}(\tau) - \frac{1}{2} \sum_{i} \left(\psi^{\dagger}_{\mathbf{n}}(\tau) \sigma_i \psi_{\mathbf{n}+\mathbf{a}_i}(\tau) + hc \right) \\ + \frac{1}{2} \sum_{i} \left(2\phi_{\mathbf{n}}(\tau) - \phi_{\mathbf{n}+\mathbf{a}_i}(\tau) - \phi_{\mathbf{n}-\mathbf{a}_i}(\tau) \right) \phi_{\mathbf{n}}(\tau) \end{array} \right\}. \tag{SI1(5)}$$

We are using convenient units where $a = v = \hbar = 1$. The Feynman rules can be read from the Fourier transform

$$A = \sum_{\mathbf{k}\omega} \left\{ \psi^{\dagger}_{\mathbf{k}\omega} \left(i\omega - \widehat{\mathbf{k}} \cdot \sigma \right) \psi_{\mathbf{k}\omega} - ie \sum_{\mathbf{p}\nu} \psi^{\dagger}_{\mathbf{k}\omega} \psi_{\mathbf{k}-\mathbf{p},\omega-\nu} \phi_{\mathbf{p}\nu} \right\} + \frac{1}{2} \sum_{\mathbf{p}\nu i} \phi^{*}_{\mathbf{p}\nu} \left(1 - \cos(p_i) \right) \phi_{\mathbf{p}\nu}. \tag{SI1(6)}$$

The fermion propagator is,

$$G_{\mathbf{p}\omega} = (i\omega - \widehat{\mathbf{p}} \cdot \sigma)^{-1} = \frac{-i\omega - \widehat{\mathbf{p}} \cdot \sigma}{\omega^2 + \varepsilon^2_{\mathbf{p}}}, \tag{SI1(7)}$$

while the photon propagator is frequency independent, $g_{\mathbf{p}\boldsymbol{\omega}} = v_{\mathbf{p}}$. The vertex is: $ie\delta_{\mathbf{k}-\mathbf{k}'+\mathbf{p}}\delta_{\omega-\omega'}$. These Feynman rules are used to calculate the linear response diagramatically.

2 Direct calculation of the conductivity tensor

2.1 General relation between conductivity tensor and the dielectric constant

We calculate the transversal and longitudinal conductivities σ_T and σ_L. From Eq.(3) we derive expression for two scalars formed from the conductivity tensor σ_{ij} :

$$\begin{aligned} 2\sigma_T(\omega, k) + \sigma_L(\omega, k) &= \sigma_{ii}(\omega) \qquad \text{(SI1(8))} \\ \sigma_L(\omega, k) &= \lim_{k \to 0} \frac{k_i k_j}{k^2} \sigma_{ij}(\omega). \end{aligned}$$

Of course, due to charge conservation the transverse conductivity is proportional to the dielectric constant (Matsubara)[1]

$$\sigma_L(\omega, k) = \frac{\omega}{4\pi} \left(1 - \varepsilon(\omega, k) \right). \tag{SI1(9)}$$

2.2 Non-interacting WSM

The ac conductivity of the non-interacting WSM on the lattice is obtained from the Kubo formula. The trace is (for positive ω)

$$\sigma_{ii}(\omega) = \frac{1}{\omega} e^2 \sum_{\mathbf{p},\nu} \mathrm{Tr}\left\{\sigma_i G_{\mathbf{p},\nu} \sigma_i \left(G_{\mathbf{p},\nu+\omega} - G_{\mathbf{p},\nu}\right)\right\} = 2e^2 \sum_{\mathbf{p}} \frac{\omega}{\varepsilon_{\mathbf{p}} \left(\omega^2 + 4\varepsilon_{\mathbf{p}}^2\right)}, \tag{SI1(10)}$$

while the longitudinal conductivity is

$$\begin{aligned} \sigma_L(\omega) &= \lim_{k\to 0} \frac{e^2}{\omega k^2} \sum_{\mathbf{p},\nu} \mathrm{Tr}\left\{\mathbf{k}\cdot\sigma G_{\mathbf{p},\nu} \mathbf{k}\cdot\sigma \left(G_{\mathbf{p},\nu+\omega} - G_{\mathbf{p},\nu}\right)\right\} \quad \text{(SI1(11))} \\ &= \frac{2}{3} e^2 \sum_{\mathbf{p}} \frac{\omega}{\varepsilon_{\mathbf{p}} \left(\omega^2 + 4\varepsilon_{\mathbf{p}}^2\right)} = \frac{1}{3}\sigma_{ii}. \end{aligned}$$

From here one deduces that $\sigma_T = \sigma_L$ and thus no nonlocal conductivity arises in the non-interacting relativistic system, see general arguments in [27].

On the lattice one obtains

$$\sigma_T^{(0)} = \sigma_L^{(0)} = \sigma_0 = \frac{e^2}{v\hbar}\omega \left(-\frac{7}{32\pi} + \frac{2}{3\pi^2}\log(\omega)\right). \tag{SI1(12)}$$

This result is consistent with [20]. The dielectric constant in leading order is

$$\varepsilon^{(0)} = e^2 \left(\frac{7}{4} - \frac{8}{3\pi}\log(\omega)\right). \tag{SI1(13)}$$

2.3 The interaction corrections:

2.3.1 The trace in Eq.(SI1(8))

The three interaction corrections to the trace of the conductivity tensor are the self energy, the vertex and the 'glasses' corrections, see Figs.2d-f,

$$\begin{aligned} \sigma_{ii}^{ver} &= \frac{e^4}{\omega} \sum_{\mathbf{pq}\nu\rho} \mathrm{Tr}\left[v_{\mathbf{q}-\mathbf{p}}\ \widetilde{\mathbf{p}}\cdot\widetilde{\mathbf{q}}\ G_{\mathbf{p},\nu} G_{\mathbf{q},\rho} \sigma_i G_{\mathbf{q},\rho+\omega} G_{\mathbf{p},\omega+\nu} \sigma_i\right]; \\ \sigma_{ii}^{se} &= -\frac{2e^4}{\omega} \sum_{\mathbf{pq}\nu\rho} \mathrm{Tr}\left[v_{\mathbf{q}-\mathbf{p}} \widetilde{\mathbf{p}}\cdot\widetilde{\mathbf{p}}\ G_{\mathbf{p},\nu} G_{\mathbf{q},\rho} G_{\mathbf{p},\nu} \sigma_i G_{\mathbf{p},\omega+\nu} \sigma_i\right]; \quad \text{(SI1(14))} \\ \sigma_{ii}^{gl} &= \frac{e^4}{\omega} v_{\mathbf{k}} \left(\sum_{\mathbf{p},\nu} \mathrm{Tr} G_{\mathbf{p},\nu} G_{\mathbf{k}+\mathbf{p},\omega+\nu}\right)^2, \end{aligned}$$

where the first term is the vertex, the second term the self energy and the third term the 'glasses' diagram. The following shorthand is useful:

$$\begin{aligned} \widehat{k_i} &\equiv \sin k_i;\ \widetilde{k_i} \equiv \cos(k_i);\ \widehat{2k_i} \equiv \sin(2k_i);\varepsilon_k = \sqrt{\widehat{\mathbf{k}}^2}; \\ \widehat{\mathbf{k}}^n &= \left\{\widehat{k_1}^n, \widehat{k_2}^n, \widehat{k_3}^n\right\},\ \widetilde{\mathbf{k}}^n = \left\{\widetilde{k_1}^n, \widetilde{k_2}^n, \widetilde{k_3}^n\right\}. \end{aligned}$$

Calculating the trace and integrating over the internal frequencies ν and ρ results in the following expressions for the three diagrams (symmetrized in $\mathbf{p}$ and $\mathbf{q}$). The vertex

$$\sigma_{ii}^{ver} = \frac{e^4}{\omega}\frac{N}{288}\sum_{\mathbf{qp}}\frac{v_{\mathbf{q}-\mathbf{p}}\left(\Xi_1+\Xi_2\right)}{\varepsilon_{\mathbf{p}}\varepsilon_{\mathbf{q}}\left(\omega^2+4\varepsilon_{\mathbf{p}}^2\right)^2\left(\omega^2+4\varepsilon_{\mathbf{q}}^2\right)^2}, \tag{SI1(15))}$$

with

$$\begin{aligned}
\Xi_1 &= -\omega^2\left\{4\ (\widehat{\mathbf{p}}\cdot\widehat{\mathbf{q}})\ \ (\widetilde{\mathbf{p}}\cdot\widetilde{\mathbf{q}})-\widehat{\mathbf{2p}}\cdot\widehat{\mathbf{2q}}\right\};\\
\Xi_2 &= 2\left\{\begin{array}{c}(\widehat{\mathbf{p}}\cdot\widehat{\mathbf{q}})\ \ \left(\widehat{\mathbf{2p}}\cdot\widehat{\mathbf{2q}}\right)+12\widetilde{\mathbf{p}}\cdot\widetilde{\mathbf{q}}-16\varepsilon_{\mathbf{p}}^2\ \widetilde{\mathbf{p}}\cdot\widetilde{\mathbf{q}}+24\widetilde{\mathbf{q}}^3\cdot\widetilde{\mathbf{p}}\\ +4\left(\widetilde{\mathbf{p}}\cdot\widetilde{\mathbf{p}}\right)\ \ (\widetilde{\mathbf{q}}\cdot\widetilde{\mathbf{q}})\left(\ \widetilde{\mathbf{p}}\cdot\widetilde{\mathbf{q}}\right)-8\left(\widetilde{\mathbf{p}}\cdot\widetilde{\mathbf{p}}\right)\ \ \left(\widetilde{\mathbf{q}}^3\cdot\widetilde{\mathbf{p}}\right)+\mathbf{p}\longleftrightarrow\mathbf{q}\end{array}\right\},
\end{aligned}$$

the self energy,

$$\sigma_{ii}^{se} = -\frac{e^4}{\omega}\frac{N}{24}\sum_{\mathbf{qp}}\frac{v_{\mathbf{q}-\mathbf{p}}}{\varepsilon_p\varepsilon_q}\left(\frac{\Xi_3+\Xi_4}{\varepsilon_p^2\left(\omega^2+4\varepsilon_p^2\right)^2}+\mathbf{p}\longleftrightarrow\mathbf{q}\right), \tag{SI1(16))}$$

$$\begin{aligned}
\Xi_3 &= \omega^2\left\{-\varepsilon_p^4\left(\widehat{\mathbf{p}}\cdot\widehat{\mathbf{q}}\right)+2\varepsilon_p^2\left(\widehat{\mathbf{p}}^3\cdot\widehat{\mathbf{q}}\right)+2\varepsilon_p^2\left(\widehat{\mathbf{p}}\cdot\widehat{\mathbf{q}}\right)-\left(\widehat{\mathbf{p}}^2\cdot\widehat{\mathbf{p}}^2\right)\left(\widehat{\mathbf{p}}\cdot\widehat{\mathbf{q}}\right)\right\};\\
\Xi_4 &= 4\varepsilon_p^2\left\{\varepsilon_p^4\left(\widehat{\mathbf{p}}\cdot\widehat{\mathbf{q}}\right)+2\varepsilon_p^2\left(\widehat{\mathbf{p}}^3\cdot\widehat{\mathbf{q}}\right)-2\varepsilon_p^2\left(\widehat{\mathbf{p}}\cdot\widehat{\mathbf{q}}\right)-3\left(\widehat{\mathbf{p}}^2\cdot\widehat{\mathbf{p}}^2\right)\left(\widehat{\mathbf{p}}\cdot\widehat{\mathbf{q}}\right)\right\},
\end{aligned}$$

and the "glasses" diagram that proportional to the square of the number of the Dirac points points,

$$\sigma_{ii}^{gl} = \frac{e^4}{\omega}\frac{4\pi N}{3}\left(\sum_p\frac{\widehat{p}_y^2\widetilde{p}_x}{\varepsilon_{\mathbf{p}}^3\left(\omega^2+4\varepsilon_{\mathbf{p}}^2\right)}\right)^2. \tag{SI1(17))}$$

The integration over the momenta is performed with the sum of the vertex and the self energy diagrams, which ensures convergence. The integral for the glasses diagram vanishes.

$$\sigma_{ii}^{(1)} = -e^4\omega\left(\frac{1}{8}+\frac{1.308}{\pi}\log\left(\omega\right)+\frac{1}{3\pi^2}\log^2\left(\omega\right)\right) \tag{SI1(18))}$$

which expressed in physical units and physical frequency is

$$\sigma_{ii}^{(1)} = -\frac{e^2\alpha N}{\hbar v 8}\omega\left[-\frac{1.308}{2}-\frac{1}{3\pi}\log\left(\frac{a\omega}{v}\right)+i\left(\frac{1}{24}+\frac{1.308}{\pi}\log\left(\frac{a\omega}{v}\right)+\frac{1}{3\pi^2}\log^2\left(\frac{a\omega}{v}\right)\right)\right]$$

2.3.2 The longitudinal conductivity via the dielectric constant, Eq.(SI1(9)):

The general expressions for the dielectric function via $\rho-\rho$ correlator can be written as $\varepsilon = 1+e^2\varepsilon^1+e^4\varepsilon^2$ with

$$\varepsilon^1 = -e^2 v_{\mathbf{k}} Tr\sum_{\mathbf{p}\nu} G_{\mathbf{p},\nu}G_{\mathbf{p}+\mathbf{k},\nu+\omega} \tag{SI1(18))}$$

and $\varepsilon^2 = \varepsilon^{ver} + \varepsilon^{se} + \varepsilon^{gl}$ where

$$\begin{aligned}
\varepsilon^{ver} &= e^4 v_{\mathbf{k}} \sum_{\mathbf{pq}\nu\rho} \mathrm{Tr} G_{\mathbf{p+k},\nu+\omega} G_{\mathbf{p},\nu} v_{\mathbf{q}} G_{\mathbf{p+q},\rho} G_{\mathbf{p+q+k},\rho+\omega} \\
\varepsilon^{se} &= -2e^4 v_{\mathbf{k}} \sum_{\mathbf{pq}\nu\rho} v_{\mathbf{q-p}} \mathrm{Tr} G_{\mathbf{p},\nu} G_{\mathbf{q},\rho} G_{\mathbf{p},\nu} G_{\mathbf{p+k},\omega+\nu} \qquad \text{(SI1(19))} \\
\varepsilon^{gl} &= \left(e^2 v_{\mathbf{k}} \mathrm{Tr} \sum_{\mathbf{p}\nu} G_{\mathbf{p},\nu} G_{\mathbf{p+k},\omega+\nu} \right)^2
\end{aligned}$$

The terms are expanded in powers of k, the trace is calculated and integrated over the internal frequencies. All the k^0 and k^1 terms vanish after integration over the internal frequencies.

The relevant terms (symmetrized in $\mathbf{p}$ and $\mathbf{q}$):

$$\varepsilon^{se} = -\frac{e^4 \pi N}{6} \sum_{\mathbf{qp}} \frac{v_{\mathbf{q-p}}}{\varepsilon_{\mathbf{p}} \varepsilon_{\mathbf{q}}} \left\{ \begin{array}{c} \left(\frac{\left(3-\varepsilon_{\mathbf{p}}^2\right)\left(\omega^2-4\varepsilon_{\mathbf{p}}^2\right)+2\left(\omega^2+12\varepsilon_{\mathbf{p}}^2\right)}{2\left(\omega^2+4\varepsilon_{\mathbf{p}}^2\right)^2 \varepsilon_{\mathbf{p}}^2} - \frac{\left[3\omega^2+20\varepsilon_{\mathbf{p}}^2\right]\widehat{(\mathbf{2p})}^2}{8\varepsilon_{\mathbf{p}}^4\left(\omega^2+4\varepsilon_{\mathbf{p}}^2\right)^2} \right) \widehat{\mathbf{p}} \cdot \widehat{\mathbf{q}} \\ -\frac{\left(\omega^2+12\varepsilon_{\mathbf{p}}^2\right)\widehat{\mathbf{p}}^3 \cdot \widehat{\mathbf{q}}}{\left(\omega^2+4\varepsilon_{\mathbf{p}}^2\right)^2 \varepsilon_{\mathbf{p}}^2} + \mathbf{p} \longleftrightarrow \mathbf{q} \end{array} \right\} \qquad \text{(SI1(20))}$$

$$\begin{aligned}
\varepsilon^{ver} &= \frac{e^4 \pi N}{48} \sum_{\mathbf{qp}} \frac{v_{\mathbf{q-p}}}{\varepsilon_{\mathbf{p}}^3 \varepsilon_{\mathbf{q}}^3 \left(\omega^2+4\varepsilon_{\mathbf{p}}^2\right)\left(\omega^2+4\varepsilon_{\mathbf{q}}^2\right)} \qquad \text{(SI1(21))} \\
&\left\{ \begin{array}{c} \left[4\varepsilon_{\mathbf{p}}^2 \varepsilon_{\mathbf{q}}^2 - \omega^2 \left(\widehat{\mathbf{p}} \cdot \widehat{\mathbf{q}}\right)\right] \left(\widehat{\mathbf{2p}} \cdot \widehat{\mathbf{2q}}\right) - 2\varepsilon_{\mathbf{p}}^2 \left\{ 2\varepsilon_{\mathbf{q}}^2 \left(\widehat{\mathbf{2p}} \cdot \widehat{\mathbf{2q}}\right) - \omega^2 \widehat{2\mathbf{q}} \cdot (\widehat{\mathbf{q}} * \widetilde{\mathbf{p}}) \right\} \\ +4\varepsilon_{\mathbf{p}}^2 \varepsilon_{\mathbf{q}}^2 \left[4\left(\widehat{\mathbf{p}} \cdot \widehat{\mathbf{q}}\right) - \omega^2\right] (\widetilde{\mathbf{p}} \cdot \widetilde{\mathbf{q}}) + \mathbf{p} \longleftrightarrow \mathbf{q} \end{array} \right\} \\
\varepsilon^{gl} &= \frac{e^4 \pi^2 N^2}{4} \left\{ \sum_{\mathbf{p}} \frac{-\varepsilon_{\mathbf{p}}^2 + \frac{1}{3}\left(\widehat{\mathbf{p}}^2 \cdot \widehat{\mathbf{p}}^2\right) + \frac{1}{12}\widehat{\mathbf{2p}}^2}{\varepsilon_{\mathbf{p}}^3 \left(\omega^2+4\varepsilon_{\mathbf{p}}^2\right)} \right\}^2 \qquad \text{(SI1(22))}
\end{aligned}$$

The numerical integration over the internal momenta results in (expressed in physical units, Matsubara frequency)

$$\varepsilon = \frac{e^2}{\hbar v} \alpha \left\{ \begin{array}{c} N\left[-0.055 + 0.023 \log\left(\frac{a\omega}{v}\right) - \frac{1}{18\pi} \log^2\left(\frac{a\omega}{v}\right)\right] \\ + \left(\frac{N}{24}\right)^2 \left[\frac{21}{32} - \frac{1}{\pi} \log\left(\frac{a\omega}{v}\right)\right]^2 \end{array} \right\}. \qquad \text{(SI1(23))}$$

and in physical frequency:

$$\varepsilon = \frac{e^2}{\hbar v} \alpha \left\{ \begin{array}{c} N\left[-0.055 + 0.022 \log\left(\frac{a\omega}{v}\right) - \frac{1}{18\pi} \log^2\left(\frac{a\omega}{v}\right) + \frac{1}{18\pi}\frac{\pi^2}{4} + i\left(0.036 - \frac{1}{18} \log\left(\frac{a\omega}{v}\right)\right)\right] \\ + \left(\frac{N}{24}\right)^2 \left[\frac{21}{32} - \frac{1}{\pi} \log\left(\frac{a\omega}{v}\right) - i\frac{1}{2}\right]^2 \end{array} \right\} \qquad \text{(SI1(24))}$$

3 Supplemental Information 2. Surface charging

3.1 Corbino geometry with a fluxon out of the center

Assume that the disk is thick enough so that the system is z translational invariant. A thin fluxon placed at distance d on the $\hat{\mathbf{x}}$ axis. The flux therefore can be represented by $\Phi(\mathbf{r}) = \alpha t \delta(\mathbf{b}); \mathbf{b} = \mathbf{r} - d\hat{\mathbf{x}}$; see Fig.6. This produces the rotational electric field

$$E_i^{sol}(\mathbf{r}) = \frac{\alpha}{2\pi b^2}\varepsilon_{ij} b_j. \tag{SI2(1)}$$

Surface charges are induced at the aperture with density $Q(\phi)$. The density is obtained from the condition that the normal component of the current on the aperture surface on the WSM side vanishes, $\mathbf{n}\cdot\mathbf{J} = \mathbf{0}$. The current is caused by the solenoidal field with conductivity σ_T and the irrotational field (induced by the surface charges) with conductivity σ_L. The irrational field (denoting the distance from a point at the surface to the observation point $\mathbf{r}$ by $\mathbf{s} = \mathbf{r} - R\mathbf{n}'$) is:

$$E_i^{irr}(\mathbf{r}) = R\int_{\phi=0}^{2\pi}\int_z \frac{s_i\, Q(\phi)}{\left(z^2+s^2\right)^{3/2}} = 2R\int_{\phi=0}^{2\pi}\frac{(r_i - Rn_i)\, Q(\phi)}{s^2}. \tag{SI2(2)}$$

Inside the semi-metal near the surface one has for its normal component (see Appendix)

$$\mathbf{n}\cdot\mathbf{E}^{irr} = 2\pi Q(\phi). \tag{SI2(3)}$$

The above condition is then

$$\sigma_T \frac{\alpha n_i}{2\pi\left|R\mathbf{n} - d\hat{\mathbf{x}}\right|^2}\varepsilon_{ij}\left(R\mathbf{n} - d\hat{\mathbf{x}}\right)_j + \sigma_L 2\pi Q(\phi) = 0, \tag{SI2(4)}$$

so that one obtains Eq.(22)

3.2 The WSM - (Ohmic) conductor circuit

The fluxon (in the $+z$ direction) is located in the center of a composite cylinder of WSM with conductivities σ_T, σ_L in the 'upper' (u) half $(0 < \phi < \pi)$ and a local conductor with Ohmic conductivity σ in the lower (d) segment $\pi < \phi < 2\pi$. Surface charges are induced at the aperture surface and at in the interface between the two materials. Their densities are determined by the condition that the normal component of the current on the aperture surface vanishes. Only the irrotational field is involved which has contributions from the two interfaces and the surface charges. The contribution from the circular surface is dominated by the local charge (see Appendix). $\Sigma(x)$ denotes the interface charge density and $Q(\phi)$ the aperture surface charge density.

In the upper segment, the WSM, the condition at the boundary is then (in the lower segment the condition is trivially fulfilled)

$$J_r = \sigma_L E_r^{irr}(R,\phi) = \sigma_L \left[2\int_{x=R}^{\infty} \frac{\mathbf{r}}{R} \cdot \frac{(\mathbf{r}-\{x,0\})\,\Sigma(x)}{(\mathbf{r}-\{x,0\})^2} + 2\int_{x=-\infty}^{-R} \frac{\mathbf{r}}{R} \cdot \frac{(\mathbf{r}-\{x,0\})\,\Sigma(x)}{(\mathbf{r}-\{x,0\})^2} - 2\pi Q(\phi) \right] |_{r=R} = 0, \tag{SI2(5)}$$

where the z integration was already performed, as in Eq.(SI2(2)). Changing $x \to -x$ in the second integral, one gets

$$\frac{2}{R}\int_{x=R}^{\infty} \Sigma(x) \left(\frac{R^2 - xR\cos\phi}{R^2 - 2Rx\cos\phi + x^2} - \frac{R^2 + xR\cos\phi}{R^2 + 2Rx\cos\phi + x^2} \right) = 2\pi Q(\phi). \tag{SI2(6)}$$

Consider the right interface. Across the interface the current is continuous. Both above and below the interface the current consists of the solenoidal (transverse) and two irrotational (longitudinal) contributions from the interface and the aperture surface. The upper is

$$J_\phi^u(x,0) = -\frac{\sigma_T \alpha}{2\pi x} + \sigma_L 2\pi\Sigma(x) + 2\sigma_L \int_{\phi'=0}^{2\pi} \frac{R\sin\phi' Q(\phi')}{x^2 + R^2 - 2xR\cos\phi'}, \tag{SI2(7)}$$

while the lower is

$$J_\phi^d(x,0) = -\frac{\sigma\alpha}{2\pi x} - \sigma 2\pi\Sigma(x) + 2\sigma \int_{\phi'=0}^{2\pi} \frac{R\sin\phi' Q(\phi')}{x^2 + R^2 - 2xR\cos\phi'} \tag{SI2(8)}$$

Equating the two, one obtains:

$$(\sigma - \sigma_T)\frac{\alpha}{2\pi x} + 2\pi(\sigma + \sigma_L)\Sigma(x) - 2(\sigma - \sigma_L)\int_{\phi'=0}^{2\pi} \frac{R\sin\phi' Q(\phi')}{x^2 + R^2 - 2xR\cos\phi'} = 0 \tag{SI2(9)}$$

These two integral equations can be solved analytically. Rewriting Eq.(SI2(8)) as

$$\kappa_T \frac{\alpha}{2\pi x} + 2\pi\Sigma(x) = 2\kappa_L R \int_{\phi=0}^{2\pi} \frac{\sin\phi Q(\phi)}{x^2 + R^2 - 2xR\cos\phi}, \tag{SI2(10)}$$

with $\kappa_T \equiv \frac{\sigma-\sigma_T}{\sigma+\sigma_L}$ and $\kappa_L \equiv \frac{\sigma-\sigma_L}{\sigma+\sigma_L}$ and substituting Eq.(SI3(7)) into the latter gives

$$\frac{\kappa_T \alpha}{2\pi x} + 2\pi\Sigma(x) = \frac{2\kappa_L}{\pi}\int_{\phi=0}^{2\pi} \frac{\sin\phi}{x^2 + R^2 - 2xR\cos\phi} \int_{x'=R}^{\infty} \Sigma(x') \left(\frac{R^2 - x'R\cos\phi}{R^2 + x'^2 - 2Rx'\cos\phi} - \frac{R^2 + x'R\cos\phi}{R^2 + x'^2 + 2Rx'\cos\phi} \right) \tag{SI2(11)}$$

The integration over ϕ on the right hand side vanishes leading to

$$\Sigma(x) = -\frac{\kappa_T \alpha}{(2\pi)^2 x}. \tag{SI3(12)}$$

This combined with Eq.(SI2(7)) leads to the result Eq.(23).

4 Appendix. The electric field at a circular aperture with an overall neutral surface charge.

A conducting cylinder with a circular aperture (radius R) is charged locally with surface charge density $Q(\phi)$, albeit overall neutral: $\int_{\phi=0}^{2\pi} Q(\phi) = 0$. We are interested in the electric field just inside the conductor at $R+\Delta$. The vector from a point on the aperture surface to the observation point $\mathbf{r} = (R+\Delta)\{\cos\chi, \sin\chi\}$ is $\mathbf{s} = \mathbf{r} - R\mathbf{n}', \mathbf{n}' = \{\cos\phi, \sin\phi\}$. The (irrotational) field is given in SI2(2).

The normal to the aperture component just inside the metal is

$$\frac{\mathbf{r}}{R}\cdot\mathbf{E}^{irr} = 2\int_{\phi=0}^{2\pi} \frac{\mathbf{r}^2 - R\mathbf{n}'\cdot\mathbf{r}}{\mathbf{r}^2 + R^2 - \mathbf{2}L\mathbf{n}'\cdot\mathbf{r}} Q(\phi) = 2\int_{\phi=0}^{2\pi} \frac{(L+\Delta)^2 - L(L+\Delta)\cos(\phi-\chi)}{L^2 + (L+\Delta)^2 - \mathbf{2}L(L+\Delta)\cos(\phi-\chi)} Q(\phi). \tag{SI2(13))}$$

After some algebraic manipulations one gets

$$\frac{\mathbf{r}}{R}\cdot\mathbf{E}^{irr} = 2Q(\chi)\int_{\phi=-\varepsilon}^{\varepsilon} \frac{(L+\Delta)^2 - L(L+\Delta)\cos(\phi)}{L^2 + (L+\Delta)^2 - \mathbf{2}L(L+\Delta)\cos(\phi)} + 2\int_{\phi=\varepsilon}^{2\pi-\varepsilon} \frac{(L+\Delta)^2 - L(L+\Delta)\cos\phi}{L^2 + (L+\Delta)^2 - \mathbf{2}L(L+\Delta)\cos\phi} Q(\phi+ \tag{SI2(14))}$$

The integral in the first term is

$$\int_{\phi=-\varepsilon}^{\varepsilon} \frac{(L+\Delta)^2 - L(L+\Delta)\cos(\phi)}{L^2 + (L+\Delta)^2 - \mathbf{2}L(L+\Delta)\cos(\phi)} = \pi + \varepsilon - 2\arctan\frac{\Delta\cot(\varepsilon/2)}{2L+\Delta}, \tag{SI2(15))}$$

and in the $\Delta \to 0$ limit $\pi + \varepsilon$. In this limit the second integral is simply $\int_{\phi=\varepsilon}^{2\pi-\varepsilon} Q(\phi+\chi)$.

Taking now $\varepsilon \to 0$ and using neutrality one has the result that the contribution from the circular surface is dominated by the local charge:

$$\frac{\mathbf{r}}{R}\cdot\mathbf{E}^{irr} = 2\pi Q(\chi). \tag{SI2(16))}$$